

RSC Advances

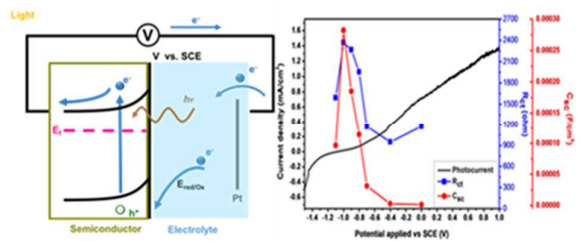


This is an *Accepted Manuscript*, which has been through the Royal Society of Chemistry peer review process and has been accepted for publication.

Accepted Manuscripts are published online shortly after acceptance, before technical editing, formatting and proof reading. Using this free service, authors can make their results available to the community, in citable form, before we publish the edited article. This *Accepted Manuscript* will be replaced by the edited, formatted and paginated article as soon as this is available.

You can find more information about *Accepted Manuscripts* in the [Information for Authors](#).

Please note that technical editing may introduce minor changes to the text and/or graphics, which may alter content. The journal's standard [Terms & Conditions](#) and the [Ethical guidelines](#) still apply. In no event shall the Royal Society of Chemistry be held responsible for any errors or omissions in this *Accepted Manuscript* or any consequences arising from the use of any information it contains.



Electrochemical impedance analysis revealed the hole-transfer step taking place directly from the valence band of AgInS₂ photoanode to the electrolyte

ARTICLE

Electrochemical Properties of AgInS₂ Photoanode Prepared Using Ultrasonic-Assisted Chemical Bath Deposition

Cite this: DOI: 10.1039/x0xx00000x

Fang-Yun Lee,^a Kai-Yu Yang^a, Yi-Chen Wang^a and Tai-Chou Lee^{a,*}Received 00th January 2012,
Accepted 00th January 2012

DOI: 10.1039/x0xx00000x

www.rsc.org/

This study focuses on preparing the AgInS₂ film electrode and studying its electrochemical properties. The AgInS₂ film after 400 °C thermal treatment had the orthorhombic structure and a direct energy band gap of 1.98 eV. The thickness of AgInS₂ film used in this study was 758.9 ± 40.9 nm. In order to understand the photoelectrochemical properties, electrochemical impedances of the AgInS₂ photoanode in response to a light intensity of 75 mW/cm² were scrutinized. It was found that homogeneous AgInS₂ films were obtained with increasing coatings. In addition, these dense films can effectively suppress the dark current. Charge transfer resistance and space charge capacitance can be retrieved from impedance spectra by fitting the experimental data to the models. In fact, Randle's model fitted the data better than other complicated models. Under illumination, the space charge capacitance and charge transfer resistance are strongly correlated to the onset of the photo-enhanced current density, suggesting a direct carrier transfer to the electrolyte from valence band of the semiconductor photoanode, rather than from the surface states.

Introduction

Ternary I-III-VI₂ compounds are direct energy-gap semiconductors, and find a wide variety of application in light emitting diodes, nonlinear optics, and photovoltaic solar cells.¹ For example, CuInS₂ and Cu(Ga:In)Se₂ are thin film solar cell materials with demonstrated efficiencies of 12.5% and 18.8%, respectively.^{3,4} The AgInS₂ is a I-III-VI₂ semiconductor with a band gap energy between 1.8 and 2.0 eV. It has a tetragonal chalcopyrite (ch-AgInS₂) structure at low temperatures and an orthorhombic (or-AgInS₂) structure at higher temperatures.⁵ AgInS₂ is considered to be a good solar cell absorber and a promising candidate to make efficient CdS/AgInS₂/CuInSe₂ tandem solar cells.⁶⁻⁸ In addition, the electrical and optical properties of AgInS₂ are dominated by donor-like defects. As a consequence, it usually exhibits n-type conductivity.¹

Recently, these ternary metal sulfide thin films, AgInS₂ and AgIn₅S₈, were used as the photoelectrode for the oxidation process⁹⁻¹². The reported photocurrent density was relatively high, in the order of few mA/cm², depending on the preparation methods, crystal structures, and applied bias. However, the detailed mechanism for the charge transfer process of this material is missing. Additionally, the anodic reaction was usually carried out in Na₂S and K₂SO₃ sacrificial reagent due to inevitable photocorrosion. As a consequence, a relatively stable

and uniform thin film electrode is required for mechanistic charge transfer investigations under illumination. Among various preparation methods, ultrasonic-assisted chemical bath deposition (UCBD) seems to be a reasonable choice. It is a simple and cost-efficient chemical process.^{13,14} The reaction takes place in the dissolved precursors generally in aqueous solution at low temperatures (30~80 °C). Our previous study showed that the photoelectrode prepared using UCBD remained intact after a course of 10 h reaction in the sacrificial reagents, only 10% drop in photocurrent density.¹⁵ The 10 h time frame should be long enough for complete mechanistic studies under illumination.

Here, electrochemical impedance spectroscopy (EIS) was used to study the charge transfer pathways in the dark and under illumination. It has been reported in the literature that useful information can be extracted from the impedance measurement by interpretation of the data with suitable physical models.¹⁶⁻²⁰ In general, for the n-type semiconductor electrode, two charge transfer routes can be assumed (here only simplified models are presented): one from valence band (Figure 1a) and the other from surface state (Figure 1b).²⁰ The recombination centers, given by R_{trapping}, trap electrons from the conduction band and holes from the valence band. If the charge transfer follows the valence band mechanism, direct charge transfer of

holes to the donor species in solution is denoted as R_{ct} (Figure 1a), whereas the surface states can also affect the charge transfer resistance, denoted by $R_{ct, trap}$ (Figure 1b). If one cannot distinguish the two capacitances, space charge capacitance (C_{sc}) and charge transfer capacitance (C_{trap}), Randle's model is usually adopted (Figure 1c).

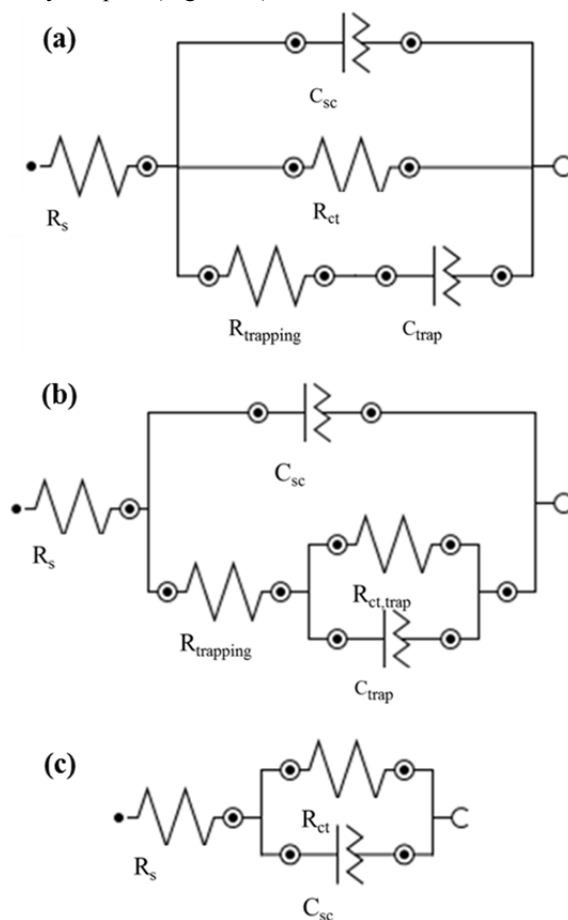


Figure 1: Equivalent circuits for the charge carrier dynamics in photoanodes. The models corresponding to (a) charge transfer dominated from the valence band, taking into account the surface states; (b) charge transfer from the surface states, (c) Randles model.

In this study, firstly we reported the deposition of $AgInS_2$ thin films on ITO-coated glass substrates using UCBD process. Results showed that thin films with the orthorhombic structure were obtained. Secondly, the EIS measurements were carried out in the dark and under illumination with various light intensities. In order to eliminate the photocorrosion that might interfere the interpretation of the data, lower light intensity of 75 mW/cm^2 was used. It was found that, one semicircle was observed for EIS measurements both in the dark and under illumination at all applied potentials, see the detailed discussion in the following paragraph. The data suggested the valence band charge transfer was the decisive pathway for the $AgInS_2$ film electrode. This finding can support the high photocurrent

density of $AgInS_2$ semiconductor materials, resulting from the efficient charge transfer of holes to the sacrificial reagents.

Experimental details

Preparation of $AgInS_2$ photoelectrode

All the chemicals in the study were used as received, without any purification process. The $AgInS_2$ semiconductor thin films were deposited on the indium tin oxide (ITO)-coated glass substrates using ultrasonic-assisted chemical bath deposition. The substrates were first cut into slides in the size of $1 \text{ cm} \times 5 \text{ cm}$. They were then cleaned subsequently in ethanol, deionized (DI) water, and acetone, respectively in ultrasonic bath for 30 minutes. Finally, the substrates were rinsed thoroughly with DI water and then dried with ultra-pure nitrogen gas.

Precursor solutions were prepared separately into two bottles. Solution A provides the metal ions, consisting of a mixture of 5 mL of 0.4 M silver nitrate ($AgNO_3$, 99% · Mallinckrodt), 5 mL of 0.08 M indium nitrate ($In(NO_3)_3 \cdot xH_2O$, 99% · Alfa Aesar), 2.5 mL of 0.4 M ammonium nitrate (NH_4NO_3 , 98%, Riedel-de Haen), and 2.5 mL of 7.4M triethanolamine ($N(CH_2CH_2OH)_3$, 99% · Sigma Aldrich). Pure sulfuric acid (95-97% · Merck) was used to adjust the pH value of the aqueous solution to around 0.5. In this Ag/In ratio, the amount of H_2SO_4 was 10 mL. Solution A was stirred for 90 min before use. Solution B contained sulfur source, which was 0.4 M thioacetamide (CH_3CSNH_2 , 99% · Merck).

The detailed experimental procedure was reported elsewhere.^{11, 21-23} A brief description was given here. 15.6 mL of Solution B poured into 4.4 mL of Solution A in a thermostat bath set at 80°C . The substrates were then vertically immersed into the precursor solution in an ultrasonic bath. The precursor solution was used immediately after preparation. The substrates were dipped for 60 min for each deposition. After the reaction, the as-deposited thin films were thoroughly washed with DI-water in an ultrasonic bath for 5 min and then dried at 100°C for 10 min to remove the loosely absorbed particles. The films were annealed in vacuum at 400°C for 1 h. The deposition process can be repeated for several times for desired thickness. Finally, the samples were then cut in halves to make each of the photoelectrode with active area of $1 \text{ cm} \times 1 \text{ cm}$. According to our previous report, the silver to indium ratio was kept at 5 to prepare $AgInS_2$ thin films. Note that the Ag/In ratio of the prepared film is different from that in the precursor solution. The detailed study can be found in the literature.²²

Materials characterizations

The morphologies of the samples and surface structures were studied using a field-emission scanning electron microscope (FEI Nova Nano SEM 230). The thicknesses of the films were determined by cross-section SEM images. The thickness of ITO was subtracted. Energy-dispersive X-ray spectrometer (EDS) attached to FE-SEM was employed to analyze the composition of the thin films. The crystal structures

of the samples were determined using Bruker D2 Phaser X-ray diffractometer. The XRD patterns were recorded in the 2θ range from 20° to 70° and at the scan rate of $2^\circ/\text{min}$. The optical properties of the films were measured using a UV-Vis spectrometer (Varian Cary 100), in the wavelength range of 400 to 800 nm at room temperature. This UV-Visible spectrometer is equipped with an integrating sphere. The transmission and reflection spectra were obtained by using an identical ITO-coated glass substrate as the reference. The optical energy band gaps of the films were determined by the absorption edges. The Raman vibrational spectra were obtained using a Thermo Fisher DXR Raman Microscope. The vibration peaks were indexed with the data reported in the literature.

Photoelectrochemical (PEC) and electrochemical impedance spectroscopy (EIS) measurements

Photoelectrochemical measurements were carried out using a standard three-electrode system, including a semiconductor thin film as the working electrode, a Pt plate electrode as the counter electrode, and a saturated calomel electrode (SCE) as the reference electrode. An aqueous solution of 0.25 M K_2SO_3 and 0.35 M Na_2S (pH = 13.3) was used as the electrolyte, which was prepared using MILLIPORE water (resistivity 18.2 $\text{M}\Omega\cdot\text{cm}$), degassing it by purging with high purity nitrogen, and then ultrasonicated for 30 min before each experiment. All the photoelectrochemical experiments were carried out under a stationary condition with nitrogen being bubbled through the electrolyte prior to and between all measurement while it was kept flowing over the solution during the measurement. A copper wire was attached to the conducting layer of the working electrode with silver paste. The back and sidewall of the samples was covered with epoxy resin to prevent current leakage. The sample was then placed in the electrochemical cell at a distance of 5 cm from the quartz window. All the samples had an area of 1.0 cm^2 . Current-voltage characteristics of the samples were obtained as a function of applied potential ($-1.5 \sim +1.0\text{ V}$ vs. SCE) and under front-side illumination with a computer-controlled potentiostat (Autolab PGSTAT302). The scan rate was set at 2.5 mV/s . A 300 W Xe lamp (Perkin Elmer Model PE300UV) with UV-cut filter ($> 400\text{ nm}$) was used as the light source. The light intensity was varied from 0 to 100 mW/cm^2 . The intensity was measured by an optical power meter (Oriel Model 70310).

The electrochemical impedance spectroscopic (EIS) experiments were carried out with the same system mentioned in the previous paragraph. In the dark, the responses were recorded by sweeping the frequencies from 10 to 10^4 Hz at a certain applied voltage (from -1.1 to 0.0 V vs. SCE). A small sinusoidal signal of 10 mV was applied in addition to the bias potential. Under illumination, the light was shined on the semiconductor side of the working electrode. At the same time, the impedance measurements were carried out. The charge transfer parameters of the samples were retrieved by fitting the experimental data to the proposed models shown in Figure 1.

Results and discussion

The basic idea of chemical bath deposition is the selective nucleation and growth on the substrate surfaces when the ion concentration products presented in the precursor solution exceed the solubility products. The mechanism of growth of binary metal sulfide thin films was discussed thoroughly. Some reviews can be found²⁴⁻²⁷. Based on our experience, the quality of the Ag-In-S thin films, prepared by normal chemical bath deposition (CBD), depends strongly on the details of the experimental conditions, e.g., humidity, chemical providers, temperature and etc. In fact, the vendor and purity of the indium nitrate is critical for repeatable results. Although good quality films can be fabricated by the CBD process, the yield is relatively low and very often the dark current density is high. We found that dense films are required to decrease the dark current density, i.e., reduce the electron-hole charge recombination and the leakage current between the substrate and the electrolyte. In order to find a solution to mitigate aforementioned problems, we have to understand the mechanism of CBD process. As stated in the literature, e.g. reference,²⁷ ion-by-ion deposition mechanism, or at least mixed ion-by-ion and cluster-by-cluster mechanism can increase the adhesion and interface properties. In such regards, ultrasonic vibration during chemical bath deposition offers a better way to make the film more homogeneous and compact.^{13, 14}

In addition, operating window for the synthesis of stoichiometric AgInS_2 is rather small, as can be seen in the $\text{Ag}_2\text{S-In}_2\text{S}_3$ phase diagram.²⁸ The single phase AgInS_2 is generated only when the ratio of Ag/In is close to one. Not surprisingly, relatively more reports regarding the preparations and characterizations of AgInS_2 thin films can be found in the literature.^{21, 22, 29-31} In this study, however, we first reported the generation of homogeneous AgInS_2 thin films. Moreover, ultrasonic-assisted chemical bath deposition (UCBD) offers another wet process to generate thin films with the orthorhombic structure. Note that AgInS_2 thin films with the chalcopyrite phase, the low temperature stable phase, were usually reported using pyrolysis and electrodeposition.^{10, 32} Secondly, electrochemical impedance can be measured in the dark and under illumination. Therefore, the charge transfer mechanism can be interpreted for this visible light-active material.

Preparation of AgInS_2 Photoanode

Based on our experience, metal ion concentrations have a profound influence.^{11, 15, 23} Additionally, other parameters, such as reaction temperature, substrate surface properties, chelating agents, and etc., must be tuned in order to obtain good quality thin films. In this study, AgInS_2 on ITO-coated glass substrate were generated when Ag/In kept at 5. Figure 2a shows the XRD patterns of the sample. Six major peaks at $2\theta = 24.992, 25.427, 26.586, 28.382, 43.692, \text{ and } 44.530^\circ$ can be assigned to the (1 2 0), (2 0 0), (0 0 2), (1 2 1), (0 4 0), and (3 2 0) planes of orthorhombic AgInS_2 (o- AgInS_2 , JCPDS 25-1328). Peaks at

30.580, 35.466, and 51.037° correspond to the diffraction from the ITO (JCPDS 06-0416) on top of the glass substrates. Figure 2b shows the Raman spectrum of the sample prepared. Three crystal vibration peaks can be clearly seen between 200 and 400 cm^{-1} . The peaks at 275, 300, and 350 cm^{-1} can be assigned to o- AgInS_2 .³³ Additionally, the spectrum shown in Figure 2b can be distinguished from that of AgIn_5S_8 . Hu et al. reported the synthesis of silver indium sulfide nanocrystals and indicated that a strong peak at 130 cm^{-1} can be assigned to AgIn_5S_8 .³⁴ The absence of the peak in our samples is evident that AgIn_5S_8 is not present in our thin films. The Raman spectrum of bare ITO was also displayed for comparison. A broad peak at 550 cm^{-1} was observed, which agrees with the data reported.³⁵ The result suggests that the surface properties of the ITO-coated substrates and the solution chemistry used in our process favor the nucleation and growth of high temperature stable orthorhombic phase.

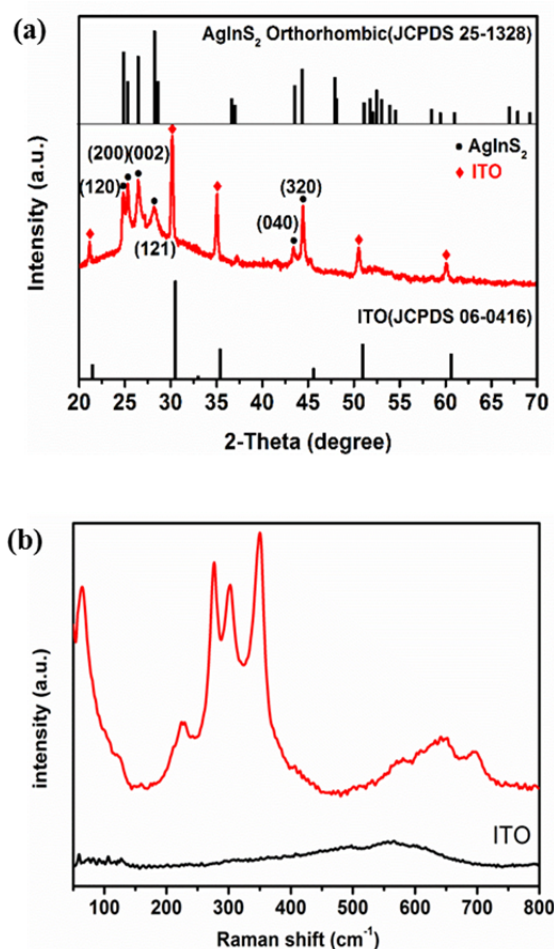


Figure 2: (a) X-ray diffraction pattern of the AgInS_2 sample, and (b) Raman spectra of AgInS_2 and bare ITO-coated glass substrate.

Figure 3 exhibits the SEM images of the surface morphology and cross-section of the sample. The low-magnification SEM image, Figure 3a, demonstrates that the AgInS_2 film covered the ITO-coated glass substrate uniformly.

In addition, the high-magnification image, Figure 3b, shows that a dense sheet-like structure were generated using UCBD process. The microstructure is similar to that previously reported.^{11, 22} From Figure 3c, the cross-sectional SEM image, the thickness was determined by averaging at least three different spots, and at least two images were used. The thickness of the sample is 758.9 ± 40.9 nm. Composition of the sample determined using EDS was Ag : In : S = 1 : 1.14 : 1.94, very close to the stoichiometric ratio of AgInS_2 . Based on the crystal structures and compositional analyses, o- AgInS_2 films were obtained using the UCBD method.

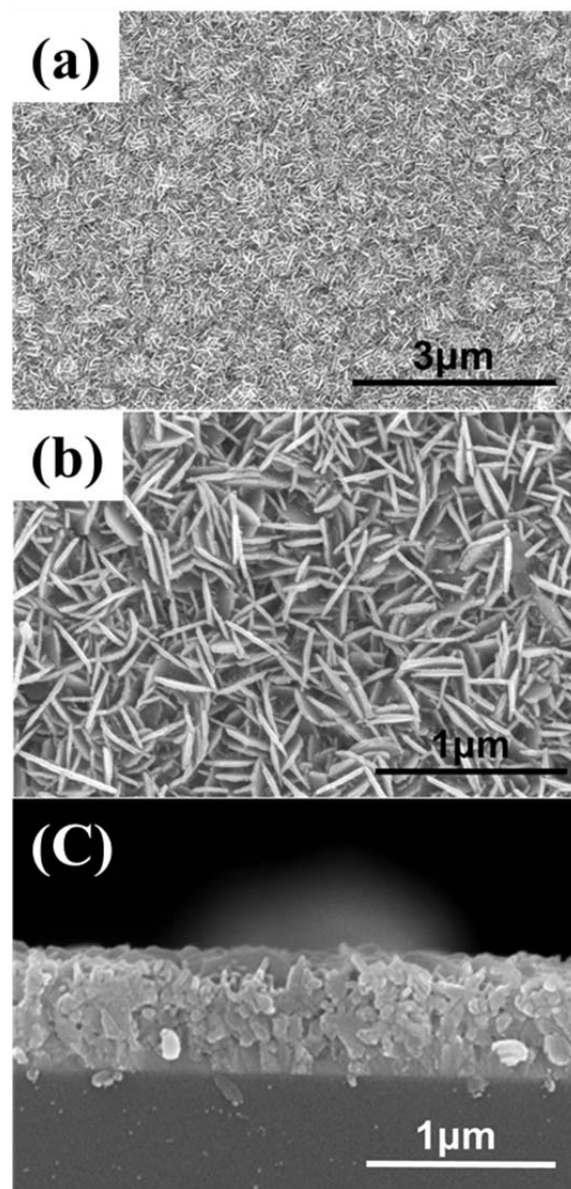


Figure 3: SEM images of top-view (a) low magnification (15K), (b) high magnification (100K), and (c) cross-section of AgInS_2 film.

The optical properties were further characterized. Figure 4 shows the transmittance and reflectance spectra recorded by UV-Vis spectrometer with an integrating sphere. The

transmission spectrum indicates that the sample exhibits a sharp absorption around 650 nm, with a relatively low reflectance (< 6%). The optical band gaps can be estimated from the absorption spectra according to the following relationship:³⁶

$$(\alpha h\nu) \propto (h\nu - E_g)^n \quad (1)$$

where $h\nu$ is the photon energy, E_g is the optical band gap, and α is the absorption coefficient which can be obtained from the following equation:

$$T(\lambda) = [1 - R(\lambda)]^2 \exp(-\alpha d) \quad (2)$$

where T is the transmission and R is the reflectance. n appeared in Equation (1) is 1/2 for direct band gap. The inset in Figure 4 plots $(\alpha h\nu)^2$ against $h\nu$. The linear extrapolation to $(\alpha h\nu)^2 = 0$ gives the optical band gap. From this figure, the direct band gap of our sample is 1.98 eV. The value is in good agreement with that reported in the literature.³⁷

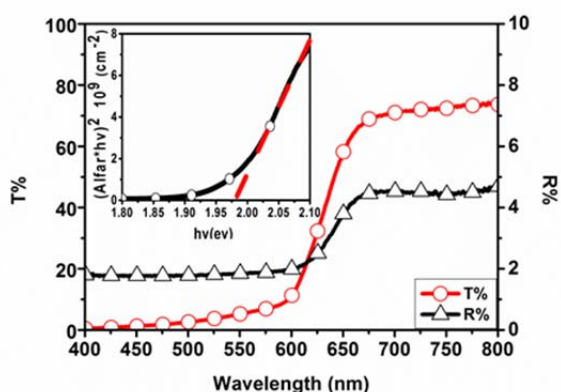


Figure 4: Transmission and reflection spectra of the AgInS₂ film. Inset: $(\alpha h\nu)^2$ vs. $h\nu$ plot for energy gap determination. Open circle: transmittance; Open triangle: Reflectance.

Electrochemical impedance analysis

The electrochemical properties of the AgInS₂ thin film immersed in the sacrificial reagent (0.25 M K₂SO₃ and 0.35 M Na₂S) were scrutinized. This sacrificial reagent was used as the hole scavenger. SO₃²⁻ and S²⁻ ions as electron donors effectively suppress the photocorrosion of the metal sulfide photocatalyst.³⁸ Our photocurrent measurements indicated that the dark current of the sample (in the order of 10⁻⁷ A/cm²) is much smaller than that of thinner samples (~10⁻⁴ A/cm²). Considering the stability of the semiconductor thin films immersed in the electrolyte, the sample (thickness of 758.9 nm) was used exclusively for the electrochemical analysis. First, the open circuit potential (OCP) of this semiconductor-electrolyte interface in the dark and under intense illumination was

measured, see Figure 5. The thin film was vertical placed in the electrolyte overnight for equilibrium. The OCP in the dark decreased gradually and reached a stable potential of -0.73 V vs. SCE. This value should be the Fermi level of the electrolyte, and the decrease in OCP might be associated with the adsorption of the ions on the semiconductor surface. On the other hand, the OCP under intense illumination were rather stable, located at -0.84 V vs. SCE, corresponding to the flat band potential of the AgInS₂ photoanode. The flat band potential obtained using OCP method is relatively more positive than that obtained using other methods, e.g. Mott-Schottly method,³⁹ perhaps due to the charge recombination and slow charge-transfer kinetics at the semiconductor-electrolyte interface.

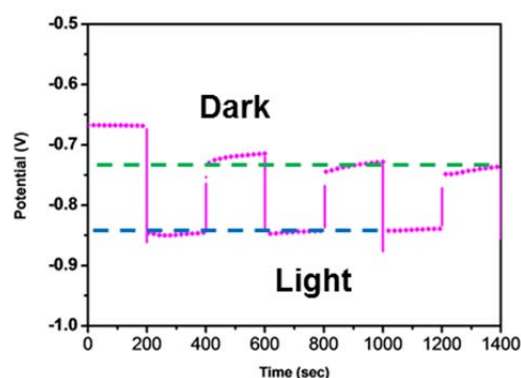


Figure 5: Open circuit potential of the AgInS₂ electrode in the dark and under intense illumination.

Figure 6 shows the Nyquist plots of the impedance measurements from -0.1 to -0.6 V vs. SCE in the dark. A typical one semicircle was observed at all potentials. Randles model, shown in Figure 1c was used to retrieve the charge transfer resistance and space charge capacitance of the semiconductor. The flat band potential was determined by plotting $1/C^2$ as a function of applied potential and extrapolate the linear part to $1/C^2 = 0$, or so called Mott-Schottly plot. From this figure, it follows that the flat band potential is approximately -1.1 V vs. SCE. The current potential measurements were carried out. Figure 7 plots the photocurrent densities of the AgInS₂ sample in response to varying light intensities, from 9 to 75 mW/cm². From this figure, the photo-enhanced current density increases with light intensity. The anodic current started to rise at approximately -1.0 V, very close to the flat band potential determined using Mott-Schottly plot. On the other hand, cathodic current appeared at approximately -1.2 V vs. SCE, both in the dark and under illumination.

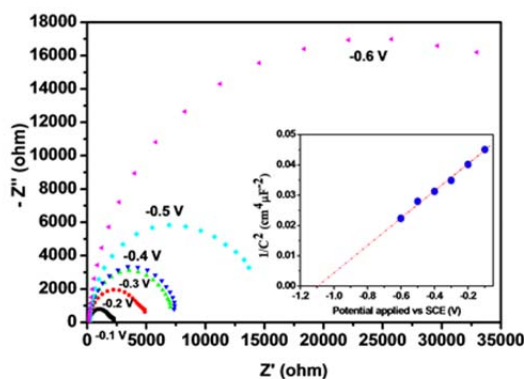


Figure 6: Nyquist plot of sample at various applied potentials in the dark. Inset: Mott-Schottky plot determined in Na₂S and K₂SO₃ sacrificial reagent.

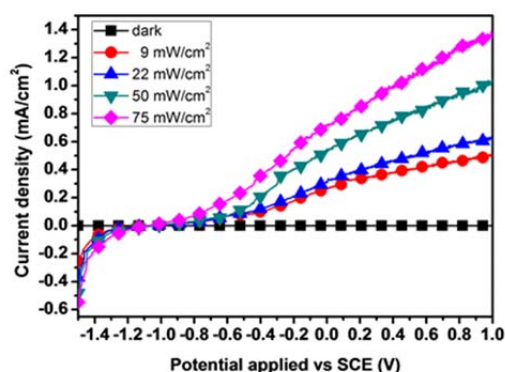


Figure 7: Current densities of sample in response to various illumination intensities from 0 (dark), 9, 22, 50, and 75 mW/cm².

The same electrochemical impedance analysis procedure can be applied to the semiconductor-electrolyte interface under illumination. Unlike the figures reported regarding the photoelectrochemical process,^{17, 20} only one semicircle was observed in our study (Figure 8a). The Nyquist plot was obtained by sweeping the frequency in the range of 10 to 10⁴ Hz. Three models were used to fit the impedance spectra under a 75 mW/cm²-illumination at various applied voltages. However, the first two models, which take the surface states into considerations, cannot give reasonable parameters, e.g. negative resistance ($R_{ct, trap}$) and zero exponent α in the constant phase element ($Z_{CPE} = Y_0(j\omega)^{-\alpha}$), appeared in Figure 1b. The simplest model, Randles circuit (Figure 1c), however, was able to derive the fit parameters from the impedance spectra. More consistent results were obtained both in the whole frequency range (10 to 10⁴ Hz) and high frequency range (10³ to 10⁴ Hz), as illustrated in Figures 8b and 8c at the applied bias of -0.9 V vs. SCE, respectively.

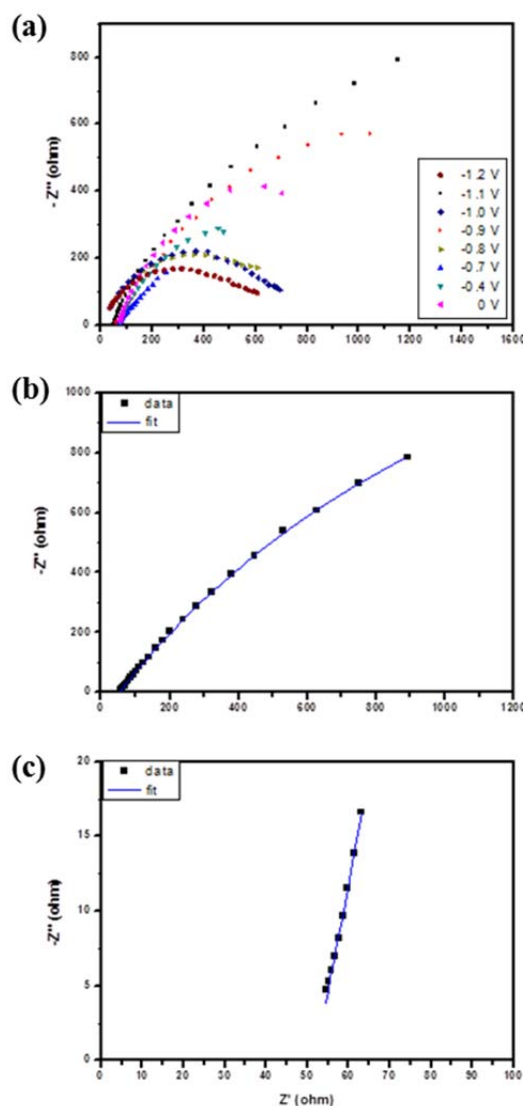


Figure 8: Nyquist plot of the sample (a) at various applied potentials measured in the frequency range from 10 to 10⁴ Hz. Detailed analysis of the sample at a bias of -0.9 V vs. SCE in the frequency range of (b) 10 to 10⁴ Hz, and (c) 10³ to 10⁴ Hz. Square: data points. Solid line: fitted curve using Randles model. All the measurements were carried out under illumination.

The charge transfer resistance and space charge capacitance in the dark and under illumination were also plotted in Figures 9a and 9b, respectively. The series resistance of the AgInS₂ film electrode in response to various bias voltages is in the range of 50 to 200 Ω , in agreement with the reported values. The charge transfer resistance in the dark is one order of magnitude larger than that under illumination. However, the resistance in the dark drops rather quickly starting from -0.6 V vs. SCE in the anodic direction, perhaps due to the Fermi level of the electrolyte and related to the oxidation kinetics from the valence band holes.²⁰ From this charge transfer resistance in

the dark and the slope estimated from the Mott-Schottky plot (Figure 6), it suggests that the AgInS₂ is relatively conductive, comparing to other photoanodes reported in the literature.^{20, 40} Note also that the charge transfer resistance under illumination peaks at -1.0 V vs. SCE, very close to the flat band potential determined previously (Figure 6 inset). This value of peak voltage coincides with the onset of the photocurrent, shown in Figure 7.

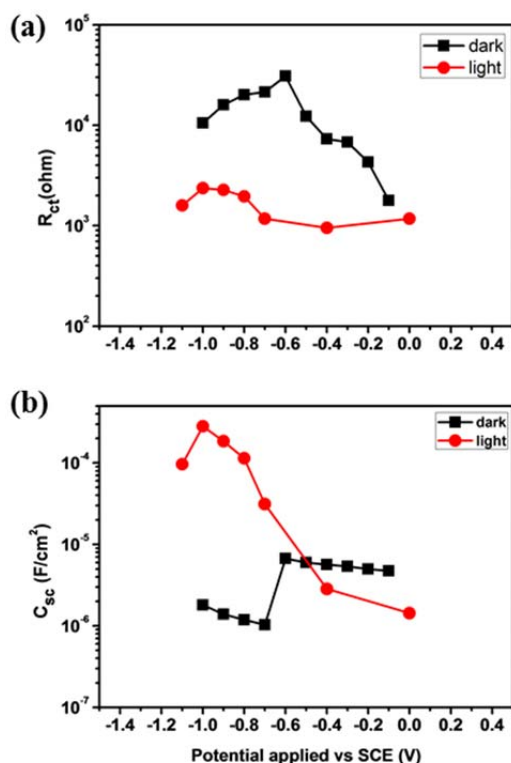
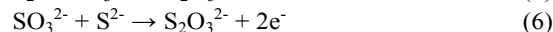
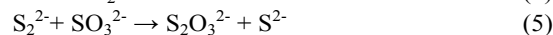
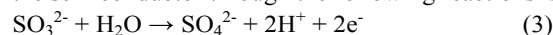


Figure 9: (a) Charge transfer resistance and (b) space charge capacitance of the AgInS₂ photoanode retrieved from EIS analysis. Square: in the dark. Circle: under illumination.

The space charge capacitances in the dark and under illumination are displayed in Figure 9a. The values for C_{sc} show a distribution behavior under illumination, following similar trend as charge transfer resistance under illumination (Figure 9b). The largest value of C_{sc} is located at -1.0 V vs. SCE, which is also very close to the flat band potential of AgInS₂ prepared in this study. However, the values of C_{sc} in the dark exhibit anomalous behavior at applied potential between -0.7 and -0.6 V vs. SCE. An order of magnitude difference in values of C_{sc} is observed. Note that this applied potential is in the vicinity of the Fermi level of the electrolyte, determined using OCP method (Figure 5). When the applied voltage is more positive than the Fermi level of the electrolyte, the space charge region is further depleted. The electrolyte used in this study is a good

electron donor. Fast electron injection from the electrolyte to the semiconductor through the following reactions is possible:³⁸



The absorption of anions and electron injections mentioned above, in the applied potential more positive than -0.6 V vs. SCE might be responsible for the increase in the values of C_{sc} observed in Figure 9b. Nevertheless, Mott-Schottky plot was also generated from the bias potentials from -1.0 to -0.7 V vs. SCE. The flat-band potential obtained was located at -1.14 V (Figure 10). However, the carrier density was lower, approximately $7.6 \times 10^{18} \text{ cm}^{-3}$, comparing to $\sim 10^{20} \text{ cm}^{-3}$ determined from the linear region between -0.6 and -0.1 V vs. SCE. The carrier concentrations agree with the values reported in the literature.⁴¹ Additionally, the positive slope from the Mott-Schottky plot indicates that the conduction of AgInS₂ prepared using UCBD is n-type.

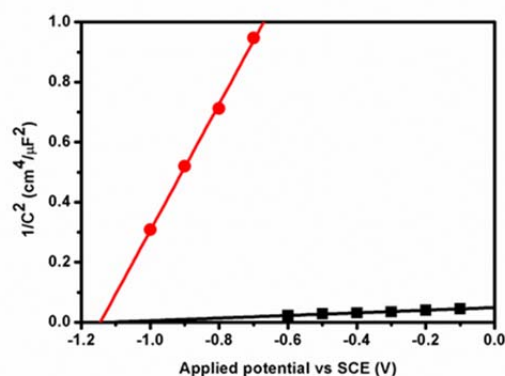


Figure 10: Mott-Schottky plot of the AgInS₂ photoanode in contact with Na₂S and K₂SO₃ electrolyte in the dark. Circle: applied potential ranging from -1.0 to -0.7 V vs. SCE. Square: applied potential ranging from -0.6 to -0.1 V vs. SCE.

The charge transfer resistance, space charge capacitance, and photocurrent density of the AgInS₂ photoanode under 75 mW/cm² illumination were plotted in Figure 11. The charging of the semiconductor right before the onset of photocurrent was revealed, as well as an increase in charge transfer resistance. To this end, through a series of systematic investigations, the mechanism for minority-carrier (hole) transfer to the electrolyte from the valence band of the semiconductor photoanode directly was suggested to be the dominate pathway. This study has demonstrated that employing electrochemical impedance analysis, important parameters can be retrieved and the charge transfer mechanism can be elucidated.

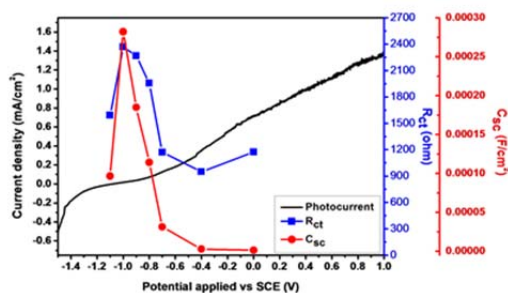
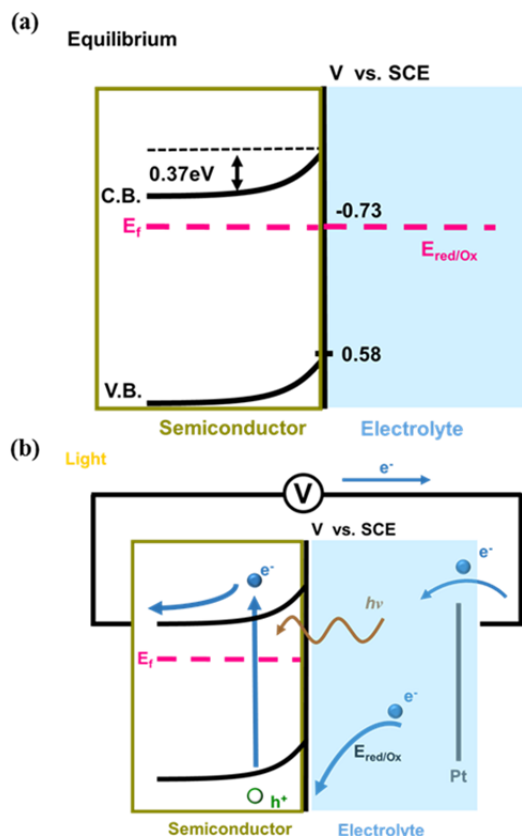


Figure 11: Photo-enhanced current density, charge transfer resistance, and space charge capacitance of AgInS₂ photoanode under 75 mW/cm² irradiation.

In summary, the relative energy levels of the conduction band and valence band of the AgInS₂ film, Fermi levels of the AgInS₂ film and the electrolyte was plotted in Scheme 1. In equilibrium (in the dark), the Fermi levels of the photoanode and electrolyte are aligned at -0.73 eV v.s. SCE. The n-type characteristic of the AgInS₂ film causes the band bending and generates a depletion layer. Under light illumination, the AgInS₂ photoanode absorbs visible light with wavelength shorter than approximately 650 nm, creating electron-hole pairs.



Scheme 1: Schematic diagram of the energy levels of AgInS₂ photoanode in the aqueous electrolyte (a) in the dark and (b) under illumination.

Electrons transport to the counter electrode (Pt) due to the electric field within the depletion layer and external applied bias. The electrolyte, containing Na₂S and K₂SO₃, injects electrons into the semiconductor as the hole scavenger. The anodic photocurrent is then observed.

Conclusions

The AgInS₂ film was generated on ITO-coated glass substrate using ultrasonic-assisted chemical bath deposition. The orthorhombic crystal structure was determined by employing XRD and Raman measurements. The photo-enhanced current density was observed in the visible light region. In addition, electrochemical impedance was employed to investigate the semiconductor-electrolyte interface, aiming to understand the charge transfer pathway of metal sulfides prepared in our laboratory. The peak position of space charge capacitance and charge transfer resistance strongly correlated to the onset of photocurrent, as illustrated in Figure 11, strongly suggesting that the hole-transfer step take place directly from the valence band. These findings may elucidate the mechanism of highly active Ag-In-S photoanodes.

Acknowledgements

The authors are grateful to the National Science Council of Taiwan for supporting this study. We thank the Instrument Center at National Central University and National Tsing-Hua University for SEM micrographs, XRD, and SIMS analysis. We also thank Professor Ya-Sen Sun's Lab at National Central University for UV-Vis and Raman measurements.

Notes and references

^a Department of Chemical and Materials Engineering, National Central University, 300 Zhongda Rd. Zhongli, Taoyuan 320, Taiwan. Corresponding author: T.-C. Lee, E-mail: taichoulee@ncu.edu.tw

1. B. Tell, J. L. Shay and H. M. Kasper, *J. Appl. Phys.*, 1972, **43**, 2469-2470.
2. S. M. Sze, in *Physics of Semiconductor Devices*, Jonh Wiley & Sons, New York, 2 edn., 1981, pp. 790-838.
3. W. Liu, D. B. Mitzi, M. Yuan, A. J. Kellock, S. J. Chey and O. Gunawan, *Chem. Mater.*, 2010, **22**, 1010-1014.
4. K. Derbyshire, in *Solid State Technology*, 2008.
5. G. Delgado, A. J. Mora, C. Pineda and T. Tinoco, *Mater. Res. Bull.*, 2001, **36**, 2507-2517.
6. S. Peng, S. Zhang, S. G. Mhaisalkar and S. Ramakrishna, *Phys. Chem. Chem. Phys.*, 2012, **14**, 8523-8529.
7. T. Sasamura, K.-i. Okazaki, A. Kudo, S. Kuwabata and T. Torimoto, *RSC Adv.*, 2012, **2**, 552-559.
8. P. Paul Ramesh, O. M. Hussain, S. Uthanna, B. Srinivasulu Naidu and P. Jayarama Reddy, *Mater. Lett.*, 1998, **34**, 217-221.
9. K.-W. Cheng, C.-M. Huang, G.-T. Pan, P.-C. Chen, T.-C. Lee and T. C. K. Yang, *Mater. Chem. Phys.*, 2008, **108**, 16-23.

10. C.-H. Wang, K.-W. Cheng and C.-J. Tseng, *Sol. Energy Mater. Sol. Cells*, 2011, **95**, 453-461.
11. W.-S. Chang, C.-C. Wu, M.-S. Jeng, K.-W. Cheng, C.-M. Huang and T.-C. Lee, *Mater. Chem. Phys.*, 2010, **120**, 307-312.
12. K.-W. Cheng, C.-M. Huang, G.-T. Pan, J.-C. Huang, T.-C. Lee and T. C. K. Yang, *J. Photochem. Photobiol. A*, 2009, **202**, 107-114.
13. Q. Liu and G. Mao, *Surf. Rev. Lett.*, 2009, **16**, 895-899.
14. A. Ichiboshi, M. Mongo, T. Akamine, T. Dobashi and T. Nakada, *Sol. Energy Mater. Sol. Cells*, 2006, **90**, 3130-3135.
15. C.-C. Wu, K.-W. Cheng, W.-S. Chang and T.-C. Lee, *J. Taiwan Inst. Chem. Eng.*, 2009, **40**, 180-187.
16. Z. Hens, *J. Phys. Chem. B*, 1998, **103**, 122-129.
17. P. Allongue and H. Cachet, *J. Electrochem. Soc.*, 1985, **132**, 45-52.
18. J. J. Kelly and R. Memming, *J. Electrochem. Soc.*, 1982, **129**, 730-738.
19. K. W. Frese, Jr. and S. R. Morrison, *J. Electroanal. Chem.*, 1979, **126**, 1235-1241.
20. B. Klahr, S. Gimenez, F. Fabregat-Santiago, T. Hamann and J. Bisquert, *J. Am. Chem. Soc.*, 2012, **134**, 4294-4302.
21. C.-H. Lai, C.-Y. Chiang, P.-C. Lin, K.-Y. Yang, C. C. Hua and T.-C. Lee, *ACS Appl. Mater. Interfaces*, 2013, **5**, 3530-3540.
22. L.-H. Lin, C.-C. Wu, C.-H. Lai and T.-C. Lee, *Chem. Mater.*, 2008, **20**, 4475-4483.
23. L.-H. Lin, C.-C. Wu and T.-C. Lee, *Cryst. Growth Des.*, 2007, **7**, 2725-2732.
24. T. P. Niesen and M. R. De Guire, *Solid State Ionics*, 2002, **151**, 61-68.
25. R. S. Mane and C. D. Lokhande, *Mater. Chem. Phys.*, 2000, **65**, 1-31.
26. K. Yamaguchi, T. Yoshida, D. Lincot and H. Minoura, *J. Phys. Chem. B*, 2003, **107**, 387-397.
27. M. Froment and D. Lincot, *Electrochim. Acta*, 1995, **40**, 1293-1303.
28. V. P. Sachanyuk, G. P. Gorgut, V. V. Atuchin, I. D. Olekseyuk and O. V. Parasyuk, *J. Alloy. Compd.*, 2008, **452**, 348-358.
29. A. F. Qasrawi, *Thin Solid Films*, 2008, **516**, 1116-1119.
30. L. Makhova, R. Szargan and I. Kononov, *Thin Solid Films*, 2005, **472**, 157-163.
31. I. V. Bodnar and V. F. Gremenok, *Thin Solid Films*, 2005, **487**, 31-34.
32. Z. Aissa, T. B. Nasrallah, M. Amlouk, J. C. Bernede and S. Belgacem, *Sol. Energy Mater. Sol. Cells*, 2006, **90**, 1136-1146.
33. S. P. Hong, H. K. Park, J. H. Oh, H. Yang and Y. R. Do, *J. Mater. Chem.*, 2012, **22**, 18939-18949.
34. J. Q. Hu, B. Deng, K. B. Tang, C. R. Wang and Y. T. Qian, *Journal of Materials Research*, 2001, **16**, 3411-3415.
35. D. Pradhan, M. Kumar, Y. Ando and K. T. Leung, *ACS applied materials & interfaces*, 2009, **1**, 789-796.
36. J. Tauc, in *Amorphous and Liquid Semiconductors*, Plenum Press, London and New York, 1974, pp. 159-220.
37. J. L. Shay, B. Tell and L. M. Schiavone, *Phys. Rev. B*, 1974, **9**, 1719-1723.
38. I. Tsuji, H. Kato, H. Kobayashi and A. Kudo, *J. Am. Chem. Soc.*, 2004, **126**, 13406-13413.
39. J. D. Beach, Jr., Ph. D., Colorado School of Mines, 2001.
40. Z. Hens and W. P. Gomes, *J. Phys. Chem. B*, 1998, **103**, 130-138.
41. K. Hattori, K. Akamatsu and N. Kamegashira, *J. Appl. Phys.*, 1992, **71**, 3414-3418.